Journal of Directed Energy, **2**, Fall 2006, 151–161

Search for Low-Absorption Regions in the 1.6- and 2.1-μm Atmospheric Windows

W. E. Bicknell,* S. Di Cecca,[1] and M. K. Griffin[2]

MIT Lincoln Laboratory, 244 Wood Street, Lexington, Massachusetts 02421

and

S. D. Swartz[3] and A. Flusberg[4]

Science Research Laboratory, 15 Ward Street, Somerville, Massachusetts 02143

Atmospheric absorption, often dominated by water vapor absorption in a naval environment, causes thermal blooming that will limit operational capability of a high-energy laser (HEL) weapon defense system. To support selection of an optimum wavelength for naval operation of an HEL and for scenario modeling, water vapor absorption in the 1.6- and 2.1-μm windows has been measured. This paper reviews the instrumentation and describes results and the impact of the measurements. It is an update of results reported at the 7th Directed Energy Symposium at Rockville, Maryland, in October 2004.

KEYWORDS: Laser beam propagation, Water vapor absorption

1. Introduction

This work was motivated by a concern for the effect of thermal blooming caused by atmospheric absorption on propagation of high-energy laser (HEL) beams that may be employed in the future as a weapon for naval defense. The concern is illustrated in Fig. 1 for an HEL onboard a vessel at a height of 10 m defending against an oncoming missile at a range of 5 km. The figure shows the achievable target intensity in a 100-cm^2 "bucket" versus laser power. Thermal blooming depends on several atmospheric conditions, which are summarized in Table 1.

The conditions correspond to a Beaufort force 5 sea with moderate waves. Figure 1 depicts the performance of lasers that operate in short-wave infrared (SWIR) atmospheric transmission windows. Atmospheric transmission windows are centered at 1.05, 1.6, and 2.1 μm, due to the relatively low water-vapor-absorption line density in these wavelength regions.

Received April 24, 2006; revision received October 2, 2006.

*Corresponding author; e-mail: bicknell@ll.mit.edu.

[1]E-mail: dicecca@ll.mit.edu.

[2]E-mail: griffin@ll.mit.edu.

[3]E-mail: sdswartz@comcast.net.

[4]E-mail: aflusberg@srl.com.

Table 1. Atmospheric parameters for the thermal blooming example of Fig. 1

Parameter	Value	Use
Wind, m/s	10	Aerosol model parameters
24-h wind, m/s	10	
Air mass parameter[a]	2	
% Relative humidity	75	Aerosol model and atmospheric absorption parameters
Pressure, mb	1,013	
Temperature, °C	20	
Crosswind, m/s	6	Thermal blooming parameter
C_N^2 $(m^{-2/3})^b$	10^{-15}	Atmospheric turbulence parameter

[a]This parameter determines the dust and so-called "B1" continental aerosol concentrations employed in the Advanced Navy Aerosol Model (ANAM4) code (available from Steve Hammel, SPAWAR Systems Center, San Diego, CA 92152).
[b]Refractive index structure constant.

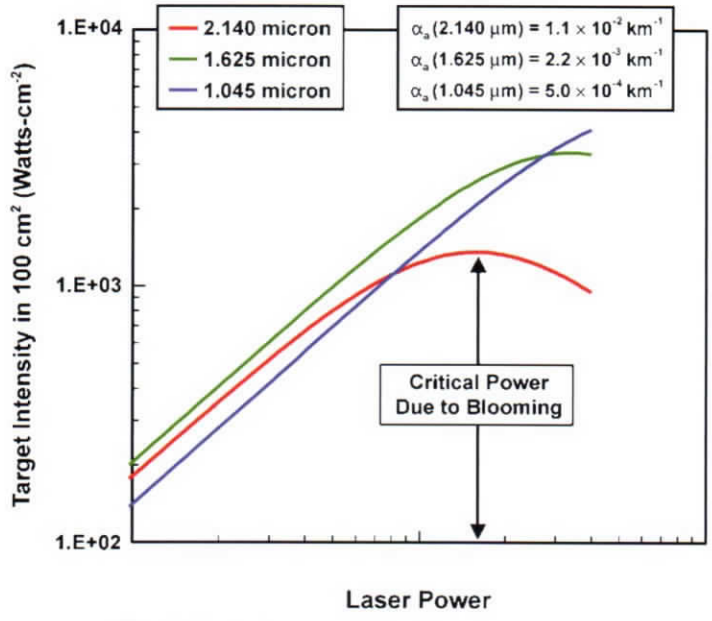

Fig. 1. Point defense scenario mode example.

It is shown in Fig. 1 that at low laser power the delivered target intensity is greater for a 2.140-μm laser than for a 1.045-μm laser, even though at 1.045 μm the absorption α_a is less than that at 2.140 μm and the far-field Airy function diffraction angle is about 50% of that at 2.140 μm (for the same aperture size). The target intensity is greater because extinction due to aerosol and molecular scattering is lower at 2.140 μm. However, as power is increased, the

2.140-μm laser reaches a critical power due to thermal blooming that limits the beam's target intensity, while the 1.045-μm laser remains unaffected. Increasing laser power at 2.140 μm beyond the critical value actually diminishes the target intensity. The critical power at 2.140 μm is solely due to the larger atmospheric absorption coefficient at that wavelength.

The 1.625-μm laser also operates in an atmospheric transmission window. The onset of thermal blooming at 1.625 μm can just be discerned at the high-power side of the abscissa of the figure.

Were it not for the effect of absorption, both the 2.140- and 1.625-μm lasers would outperform the 1.045-μm laser in terms of target intensity. Target intensity limited by scattering extinction can, in principle, be overcome by operating a sufficiently high-power HEL. However, thermal blooming caused by absorption sets a critical power that fundamentally limits the amount of target intensity delivered at any wavelength, irrespective of HEL power.

To reliably deliver lethal target intensities over varying atmospheric conditions, an HEL should operate at a wavelength nominally having low absorption, which is the subject of this investigation. With the development of the free-electron laser (FEL) for Navy applications,[8] there is a need to identify an optimum wavelength, or a set of optimum wavelengths, for operation that have minimum absorption. The 1.05-, 1.6-, and 2.1-μm window SWIR regions are candidates for FEL operation. An analysis using the Line-by-Line Radiative Transfer Model (LBLRTM) code[3,†] shows that, in these window regions, wavelengths exhibiting minimum absorption tend to lie between moderately well separated water vapor absorption lines. Absorption between moderately well separated water vapor lines is usually dominated by the water vapor continuum.[1,4]

Water vapor continuum absorption can be viewed as the contribution to absorption due to the wings of the very many water vapor vibration–rotation absorption line resonances existing on either side of a wavelength, even though the wavelength may be between two neighboring resonance lines. The strength of absorption from the continuum depends on both self-collisions and foreign (e.g., N_2) collisions between and with water vapor molecules. In the 1.6- and 2.1-μm windows, the self-collision process (between water vapor molecules) is dominant.

In 1991 measurements of the water vapor continuum at 1.056 μm were reported that found the continuum model at the time-predicted absorption to be larger than measured by about two orders of magnitude.[5] The measurement was used to modify the water vapor continuum model in the 1.05-μm-wavelength region.[2] The work reported here was motivated by an interest in investigating water vapor absorption in the 1.6- and 2.1-μm windows to ensure that no surprises arose in the choice of FEL operating wavelengths in those windows due to an experimentally unverified model of continuum absorption.

2. Instrument Description

For the investigation, Science Research Laboratory (SRL) built an instrument similar to the one used for the 1.056-μm measurements reported in 1991. Figure 2 shows a block diagram of its components.

A cell was used to hold the gas being tested. The cell was in the path of both arms of a Mach–Zehnder interferometer. A probe laser beam operating at 0.532 μm passed through

†The LBLRTM code is available from Atmospheric and Environmental Research, Inc., 131 Hartwell Avenue, Lexington, MA 02421.

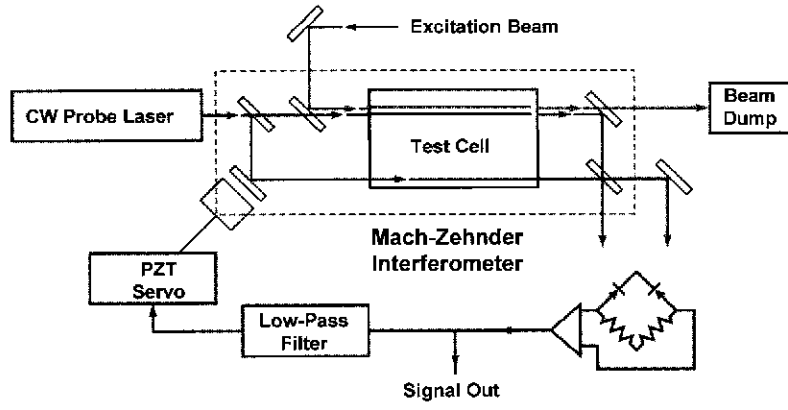

Fig. 2. Absorption measurement instrument.

the interferometer, and a fringe-shift detector sensed the path length difference between the two arms. An excitation laser beam also passed through the cell and was coaligned with one interferometer arm. The excitation laser was tunable over both the 1.6- and 2.1-μm window wavelength regions.

Absorption of the excitation laser beam caused the gas to heat. Heating of the gas in the excitation beam arm caused the gas to change density and, thereby, change the overall optical path difference (OPD) of that arm. The probe beam's fringe shift detector sensed this change in OPD between the two arms. By calibrating the detector, a very small absorption (2×10^{-4} km^{-1}) was measured. An important feature of this calorimetric–interferometer technique is that it was a sensitive measurement of absorption while being insensitive to molecular scattering loss.

Figure 3 shows a rendition of the optical setup. The equipment was placed on an optical bench.The excitation beam was derived from the Raman-shifted output of a tunable (0.73–0.79 μm), Light Age[‡] alexandrite, 15-pulse/s (pps) Q-switched, flash lamp pumped laser. Etalons were used to obtain a pulse full-width, half-maximum (FWHM) spectral line width of $\approx$2 cm^{-1} ($\approx$0.0005 μm at 1.6 μm and $\approx$0.0009 μm at 2.1 μm). The scanning step size was 1.7 cm^{-1}, which was comparable to the FWHM spectral linewidth. The Raman-shifted FWHM pulse duration was 50 ns. Light Age also built the Raman cells that used high-pressure methane and hydrogen gas. The interferometer was supported above the surface of the optical bench by a low-frequency resonant spring suspension system. The mechanical support system for the Mach–Zehnder interferometer was designed to render it insensitive to translation, rotation, horizontal bending, and torsion perturbations, but weakly sensitive to vertical bending disturbances.

The equipment was computer controlled with user-friendly Lab View[§] software developed by SRL that automated wavelength scan and data collection operation. Typically, tens to several hundred excitation laser pulses were averaged at each wavelength during a scan to measure an absorption spectrum. A quick-look presentation of averaged pulse data was available for immediate review of a scanned absorption spectrum, while measured data

[‡]Light Age, Inc., 500 Apgar Drive, Somerset, NJ 08873.

[§]Lab View code is available from National Instruments, 11500 N. Mopac Expressway, Austin, TX 78759.

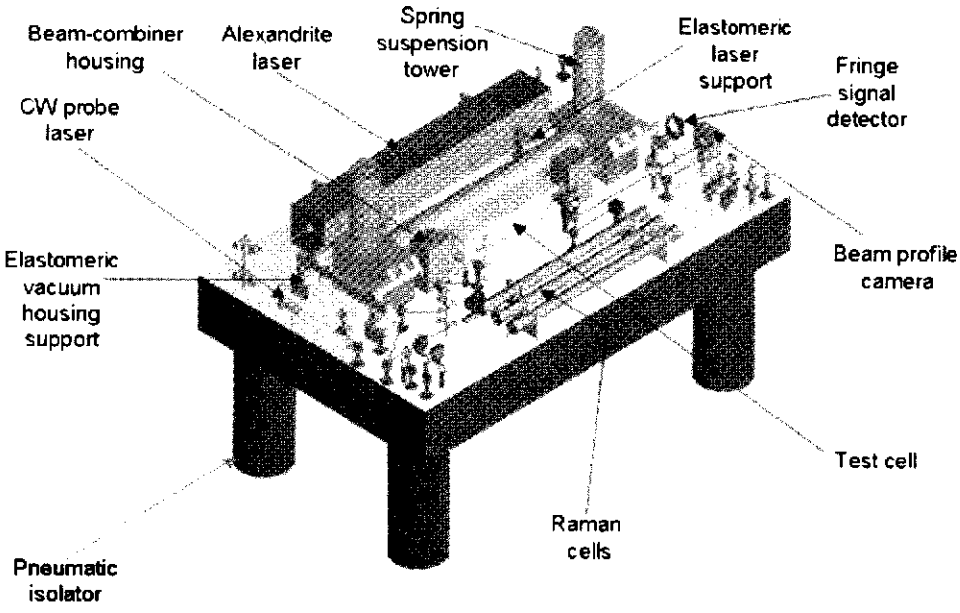

Fig. 3. Drawing of optical bench setup.

from each individual pulse were recorded in a MATLAB[¶] file format for later review and analysis.

After construction, the equipment was operated at SRL for about eight months and then delivered to MIT Lincoln Laboratory and operated there for about two months. At SRL ancillary equipment such as the laser power supply and vacuum pumps were operated in a separate room next to the optical bench. For the first month of operation at MIT Lincoln Laboratory, a vacuum pump was operated next to the optical bench, causing a somewhat elevated acoustic and vibration noise environment.

3. Instrument Performance

The instrument proved capable of 2×10^{-4} km^{-1} absorption coefficient 1σ precision in both the 1.6- and 2.1-μm windows. The instrument was used to measure absorption over the dynamic range of 10^{-3}–10^{2} km^{-1}. Calibration of the instrument in both the 1.6- and 2.1-μm windows was based on LBLRTM line strengths of methane given in the high-resolution transmission molecular database (HITRAN).[7] Research-grade methane and nitrogen were used in calibrations.

At MIT Lincoln Laboratory the linearity response in the 2.1-μm window was examined in some detail. Figure 4 shows the result of one test. Methane pressure was varied from 8 to 0.009 torr while the total pressure was maintained at 760 torr using a nitrogen backfill. The test effectively varied the methane concentration, to which the absorption coefficient is proportional, over about four orders of magnitude.

[¶]MATLAB code is available from The Math Works, Inc., 3 Apple Hill Drive, Natick, MA 01760.

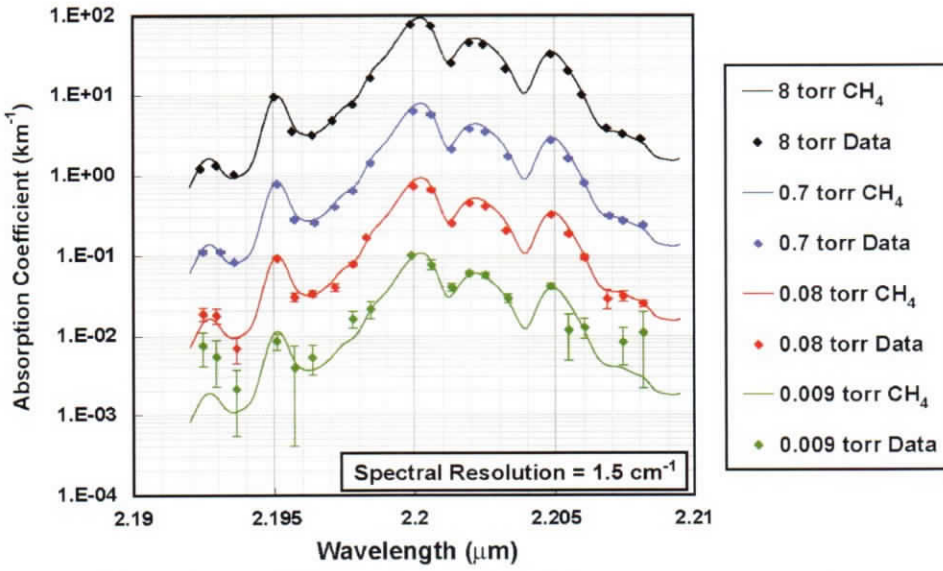

Fig. 4. 2.1-μm window large dynamic range measurements with CH_4.

The procedure was to sequentially pump the nitrogen-plus-methane gas mixture down to 76 torr and then fill the cell back up to 760 torr with nitrogen. The solid curves are the fit of the data to LBLRTM code predictions. In this case, each scan run was repeated four times, allowing an estimate of the repeatability of the measurements. The error bars shown on the data indicate the scatter in the four measurements. At some wavelengths and at low methane pressure the scatter was significant compared with the absorption value measured. Figure 5 is a plot of the data in Fig. 4 with the 8-torr values taken as unity. The figure indicates that the response is linear except for deviation at lower methane concentrations.

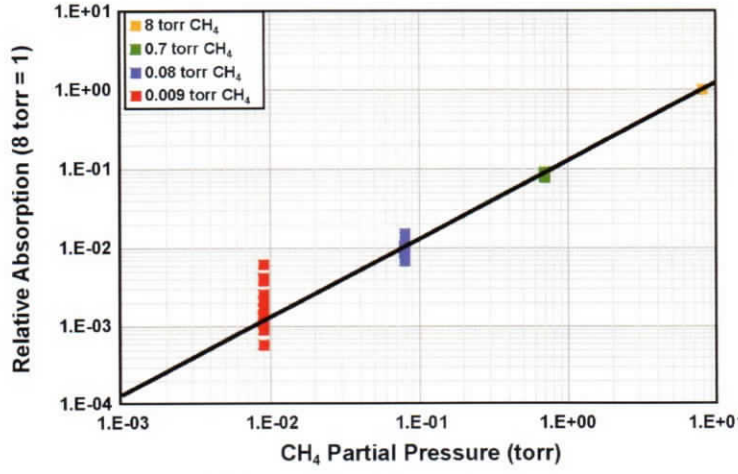

Fig. 5. Linearity versus absorption.

The repeatability, a limit of measurement accuracy at low absorption, was traced to an approximately 500-Hz resonance in the interferometer support or suspension structure that had a "Q" of about 80. The acoustic impulse generated by the firing flash lamps in the alexandrite laser next to the cell and the vacuum pump appeared to induce a random-phase, 500-Hz pedestal on the measured signal. The pedestal varied from pulse to pulse. Signal processing provided a least-mean-square (LMS) fit to a random pedestal signal that varied up to quadratically in time. The LMS fit to the pedestal was subtracted from the measured signal, eliminating up to a quadratic component of error. However, the LMS fit to the pedestal left, on average, a small residual. The uncorrectable residual component varied from scan to scan, thus affecting the repeatability of the measurements. The lack of repeatability became noticeable at small absorption coefficient values.

The source of the 500-Hz resonance was not determined. However, it may have been the result of an unpredicted resonance in the low-frequency spring support structure that holds the interferometer mount off the optical bench or, possibly, due to the weak sensitivity of the mechanical interferometer mount to a resonance of a vertical bending mode. Other than the effect of repeatability at low absorption values, the linearity of the instrument over a large dynamic range was satisfactory.

Figure 6 is a scatterplot of the data from Fig. 4. It shows the uncertainty in the measured absorption coefficient versus mean absorption coefficient. For absorption coefficients greater than about 10^{-1} km^{-1}, the uncertainty appeared to be approximately proportional to the absorption coefficient. The uncertainty ranged from about 1% of the coefficient at large absorption values to about 3.5% near a coefficient of 10^{-1} km^{-1}.

For absorption coefficients less than 10^{-1} km^{-1}, the uncertainties varied measurement to measurement essentially independently of the value of the absorption coefficient. The average value of the uncertainties in this regime was about 3.5×10^{-3} km^{-1}. The variation in the uncertainties for low absorption coefficient values appeared to be random. By averaging 10 or more scans, the uncertainty in the averaged scan values were reduced to about 10^{-3}km^{-1}.

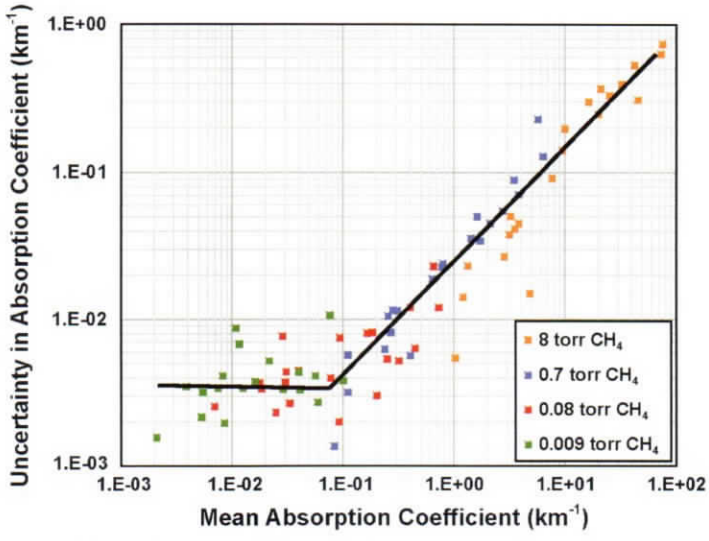

Fig. 6. Repeatability versus absorption coefficient.

At SRL, measurements were made in both the 1.6- and 2.1-μm windows. There, the minimum averaged uncertainty at low absorption values was about 5×10^{-4} km^{-1} or a factor 2 less than at MIT Lincoln Laboratory. The lower measurement repeatability floor at SRL may have been due to a difference in room acoustics or the absence of a vacuum pump near the instrument.

4. Measurements

Early measurements made at SRL included a survey of the 2.1-μm water vapor window near an optimum FEL operating wavelength predicted by LBLRTM. Optimum FEL operating wavelengths depend on the FWHM spectral width of the FEL output pulse train. An FEL can be operated with a narrow ($\Delta\nu = 14$ cm^{-1}), medium ($\Delta\nu = 27$ cm^{-1}), or broad ($\Delta\nu = 95$ cm^{-1}) pulse spectrum, depending on the phasing of the bunched electron beam with the wiggler.[6] The region surveyed was from 2.09 to 2.19 μm. The predicted optimum wavelength region for narrow operation was 2.143 μm. The measurements verified that a minimum in absorption did, indeed, occur at 2.143 μm. Also, based on calibration with methane, the peak water vapor line strengths appeared to be in good agreement with the HITRAN database.

At SRL, measurements were made in the 1.6-μm water vapor window, one of the most interesting of which is shown in Fig. 7. The measurement covered the wavelength interval of 1.624–1.635 μm. LBLRTM predicted optimum wavelengths for the narrow, medium, and broad spectral width FEL operation that ranged from 1.623 to 1.626 μm, which is close to, or overlapping, the measured interval. The interesting result uncovered was that, between well-separated water vapor lines in this wavelength region, the observed absorption was considerably larger than predicted. As indicated in Fig. 7, an LBLRTM calculation showed that the water vapor continuum value would have to be increased by about a factor of nine to accommodate the observed absorption. That is, the water vapor continuum absorption predicted by LBLRTM is about a factor of nine times too small.

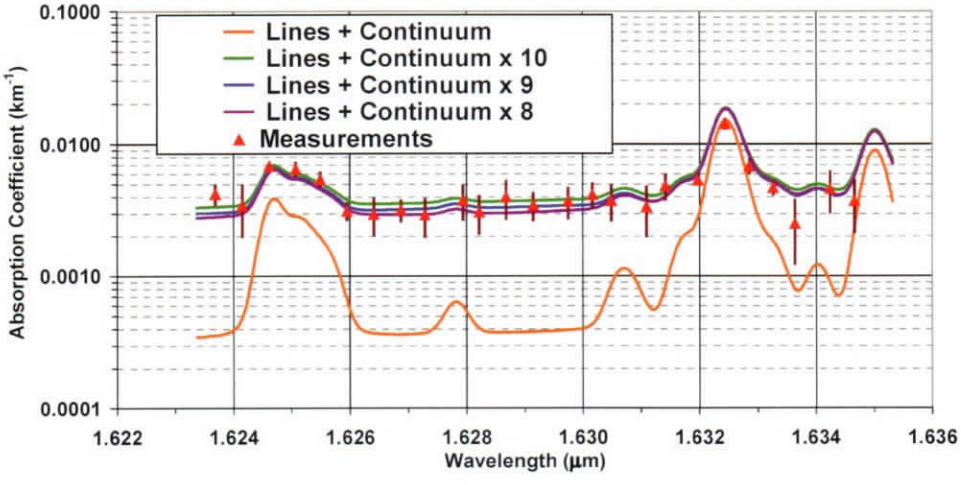

Fig. 7. 1.6-μm H_2O vapor measurement.

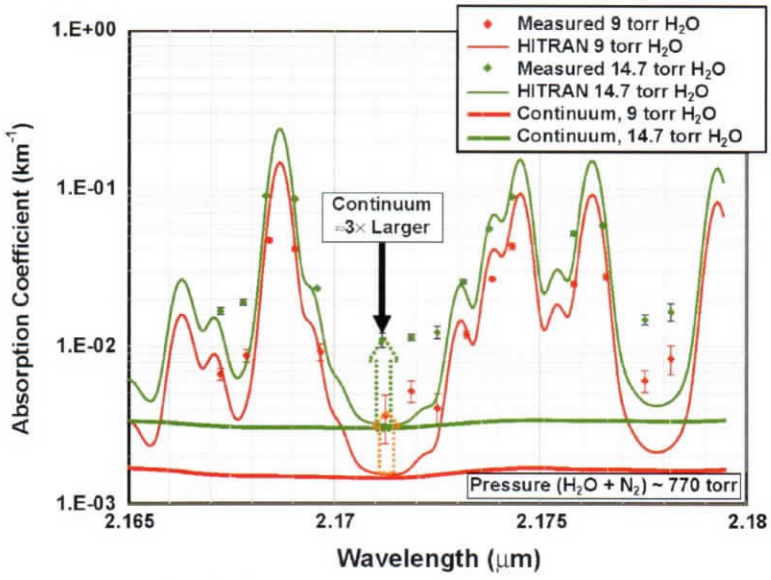

Fig. 8. 2.1-μm H_2O vapor measurement.

Absorption in the 2.1-μm window was revisited after delivery of the equipment developed by SRL to MIT Lincoln Laboratory. The result is shown in Fig. 8 for measurements in the wavelength interval of 2.165–2.180 μm. This wavelength interval does not encompass the LBLRTM predicted minimum absorption wavelength at approximately 2.14 μm for narrow and medium FEL wavelengths, but was sufficiently close to be of interest considering the relatively slow variation of water vapor continuum absorption with wavelength. The figure depicts measured values and an LBLRTM fit to the data for two water vapor partial pressures. An interesting result is observed for both water vapor partial pressures at 2.1712 μm, which is between well-separated water vapor absorption lines. There, the observed absorption is about three times larger than predicted. The figure shows that at 2.1712 μm the absorption predicted by LBLRTM is entirely due to the water vapor continuum. The data indicate that the LBLRTM prediction of the water vapor continuum is about a factor of three too small.

An estimate of the accuracy of these observations is important. The uncertainties in the factors for the underestimation of the water vapor continuum absorption by the current LBLRTM code for the 1.6- and 2.1-μm windows, respectively, depend on the uncertainties in both the measurement (factor's numerator) and the LBLRTM prediction (factor's denominator).

The uncertainty in the numerator, which is the measured value, is primarily due to the repeatability. The 1σ value for this was taken to be 14% for the1.6-μm and 10% for 2.1-μm measurements. Although the uncertainty in the observation due to repeatability was smaller at 1.6 μm than at 2.1 μm, so was the value of the observed absorption, thus giving a slightly larger percentage uncertainty. The uncertainty in the denominator is primarily due to uncertainties in measurement conditions, such as temperature, pressure, and relative humidity, and the effect of these on the prediction of the LBLRTM code. This 1σ uncertainty was taken to be about 10% for measurements in both windows. The numerator and denominator 1σ uncertainties were root-sum-squared, doubled to provide a 95% confidence level estimate,

and rounded to the nearest 5% value. The resulting 95% confidence levels in the factors were ±35% (±2σ) for the 2.1-μm window and ±30% (±2σ) for the 1.6-μm window.

It is of interest to note that the measurement of absorption between water vapor lines, compared to measurement of absorption at the peaks, is by and large independent of the overall calibration accuracy obtained using methane. Thus, the conclusions would be similar, even if methane line strengths in the window regions were not very well known in HITRAN.

5. Effect of Increased Water Vapor Continuum Absorption

The effect of an increased water vapor continuum absorption in the two windows was modeled using LBLRTM. It was assumed that molecular absorption is dominant or, at least, significant compared to weakly wavelength-dependent aerosol absorption. The results for the minimum absorption operating wavelengths for 95% relative humidity at 25°C are summarized in Table 2.

Results are shown for the narrow, medium, and broad FEL spectral width operating modes. For the 1.6-μm window the absorption is increased by factors of 3.24, 3.05, and 1.86 for the narrow, medium, and broad spectral widths, respectively. For the 2.1-μm window the absorption is increased by factors of 1.70, 1.42, and 1.65 for the narrow, medium, and broad spectral widths, respectively. The seemingly anomalous behavior of the broad spectral width factor in this window is likely due to the location of the absorption minimum differing by ~200 cm^{-1} relative to the minimum of the medium and narrow.

These increases in absorption are not large enough to eliminate interest in the 1.6- and 2.1-μm window regions for HEL applications, but will have a noticeable effect on the estimated critical power and performance predictions in high-humidity conditions typical of many naval engagements.

Table 2. Effect of increased continuum absorption at minimum absorption operating wavelengths in the 1.6- and 2.1-μm windows for 95% RH and 25°C

	Continuum		
Window	Narrow	Medium	Broad
1.6 μm		×1	
α_{min}, km^{-1}	1.60×10^{-3}	1.84×10^{-3}	4.53×10^{-3}
λ_{min}, μm	1.623	1.625	1.626
1.6 μm		×9	
α_{min}, km^{-1}	5.19×10^{-3}	5.62×10^{-3}	8.43×10^{-3}
λ_{min}, μm	1.622	1.624	1.623
2.1 μm		×1	
α_{min}, km^{-1}	9.96×10^{-3}	16.4×10^{-3}	29.0×10^{-3}
λ_{min}, μm	2.143	2.140	2.250
2.1 μm		×3	
α_{min}, km^{-1}	16.9×10^{-3}	23.3×10^{-3}	47.8×10^{-3}
λ_{min}, μm	2.143	2.140	2.245

6. Summary

An instrument was built and used to measure water vapor absorption in the 1.6- and 2.1-μm atmospheric transmission windows. The instrument obtained a precision of 0.2×10^{-3} km^{-1} and operated over a dynamic range of 10^{-3}–10^{2} km^{-1}. A measurement repeatability of $(0.5–1.0) \times 10^{-3}$ km^{-1} was obtained in the 2.1-μm window and 0.5×10^{-3} km^{-1} in the 1.6-μm window.

Water vapor line intensities were confirmed to agree with the HITRAN database, and the optimum 2.1-μm operating wavelength predicted by LBLRTM was verified.

The water vapor continuum absorption was found to be larger than predicted by LBLRTM by a factor of $9\times\pm$ 35% ($\pm 2\sigma$) in the 1.6-μm window and a factor of $3\times\pm$ 30% ($\pm 2\sigma$) in the 2.1-μm window. Finally, an assessment of the effect of the increased water vapor continuum absorption on the optimum FEL operating wavelengths in the two windows was illustrated.

7. Acknowledgments

This work was sponsored by the U.S. Navy (HEL Joint Technology Office, Albuquerque, New Mexico; Program Manager Dr. Sadegh Siahatgar, PMS 405, Naval Sea Systems Command, Washington Naval Yard, Washington, DC) under Air Force Contract FA8721-05-C-0002. Opinions, interpretations, conclusions, and other recommendations are those of the authors and are not necessarily endorsed by the U.S. Government. The authors acknowledge the helpful advice of Paul Berger of MIT Lincoln Laboratory during this effort, contributions to the design of the instrument by Stephen Fulghum of SRL, and the craftsmanship of Dan Pham of SRL during the fabrication of the instrument at SRL and the setup of the equipment at MIT Lincoln Laboratory.

References

[1]Bicknell, W.E., and P.L. Kelley, "Understanding the AER-RTWG Atmospheric Optical Model," Project Memo. 107PM-LAAMS-0002, MIT Lincoln Laboratory, 22 November 2004.

[2]Clough, S.A., Atmospheric and Environmental Research, Inc., private communication (2005).

[3]Clough, S.A., and M.J. Iacono, J. Geophys. Res. **100**, 16,519 (1995).

[4]Clough, S.A., F.X. Kneizys, and R.W. Davies, Atmos. Res. **23**, 229 (1989).

[5]Fulghum, S., and M. Tilleman, J. Opt. Soc. Am. B **8**, 2401 (1991).

[6]Neil, G., Jefferson Laboratory, Newport News, VA, private communication (2002).

[7]Rothman, L.S., A. Barbe, D. C. Benner, L.R. Brown, C. Camy-Peyret, M.R. Carleer, K. Chance, C. Clerbaux, V. Dana, V.M. Devi, A. Fayt, J.-M. Flaud, R.R. Gamache, A. Goldman, D. Jacquemart, K.W. Jucks, W.J. Lafferty, J.-Y. Mandin, S.T. Massie, V. Nemtchinov, D.A. Newnham, A. Perrin, C.P. Rinsland, J. Schroeder, K.M. Smith, M.A.H. Smith, K. Tang, R.A. Toth, J. Vander Auwera, P. Varanasi, and K. Yoshino, J. Quant. Spectrosc. Radiative Transfer **82**, 5 (2003).

[8]Saulter, Q., 7th Annual Directed Energy Symposium, Rockville, MD, 18–21 October 2004.